# Analytical model for tilted coils in eddy-current nondestructive inspection

**Article** *in* IEEE Transactions on Magnetics · October 2005

DOI: 10.1109/TMAG.2005.854331 · Source: IEEE Xplore



**1 author:**

Theodoros Theodoulidis
University of Western Macedonia
**118** PUBLICATIONS **2,003** CITATIONS

# Analytical Model for Tilted Coils in Eddy-Current Nondestructive Inspection

Theodoros Theodoulidis, *Member, IEEE*

Energy Department, West Macedonia University, Kozani 50100, Greece

**The electromagnetic field and impedance of a cylindrical eddy-current probe coil are calculated analytically for arbitrary coil orientation above a conductive half-space. The remarkably simple closed-form expressions are provided as a function of coil tilt angle. The effect of tilt on the impedance change produced by a long crack is also investigated by combining the analytical model with an existing thin-skin theory for surface crack inspections. Results for both cracked and uncracked conductors are expected to be useful for evaluation of movement-generated noise in eddy-current inspections.**

***Index Terms*—Coil tilt, crack inspection, eddy currents, eddy-current testing, impedance calculation.**

## I. Introduction

MANY researchers have studied the problem of eddy-current induction by an air-cored coil above a planar conductor and derived expressions for arbitrary coil shape and position; see [1] for a survey of papers on the subject. However, these expressions are general and contain a source term that has to be calculated in order to make the model specific to a particular coil geometry and orientation [2]. Such a calculation usually requires evaluation of a double integral expansion over the coil volume and it can be done with moderate effort for simple coil shapes and coil orientations [3]–[8] and for filamentary coil loops [9]–[12]. Otherwise, for complex shapes and asymmetric coil orientations it is cumbersome to calculate analytically. In these cases, we can resort to a numerical computation of the source term [13] or to other computationally demanding universal numerical models such as three-dimensional finite-element method (3-D FEM) [14], [15].

For a cylindrical coil, which is the most common eddy-current probe design, the source term has a closed-form expression when the coil is either parallel or perpendicular to the conductor surface. In this paper, we derive such an expression for arbitrary coil orientation. The analysis is based on a previously published result for the magnetic field of a tilted filamentary circular loop [10], [11] and the use of superposition. Knowledge of the source term for the cylindrical coil makes possible the calculation of the electromagnetic field and impedance change of the coil due to the conductor. The remarkably simple expressions are provided as a function of tilt angle and can be used for parametric studies since they are rapidly computed.

The theoretical results are expected to be useful in a number of ways, including the fast computation of the incident field required by numerical methods such as the volume integral method (VIM) when simulating the case of a flaw in the conductor. Such incident fields are routinely computed for parallel coils, that is coils without tilt, and are numerically approximated for other coil orientations. Although we do not implement VIM, we nevertheless demonstrate how the presented model can be used in flaw inspections by using the closed-form expression for the incident magnetic field in a thin-skin model (high-frequency regime) [16] for an infinitely long crack. The proposed model for computing the incident field from a tilted coil is exact and the thin-skin model has been shown from previous studies to agree with experiment to about 5%. By combining the two models, we have a fast and reasonably accurate analytical tool that can assist in understanding the acquired eddy-current test signals under conditions of tilt and, thus, evaluate the effect of movement-generated noise on the useful flaw signal.

Probe tilt is identified as the major source of noise in eddy-current surface inspections [14], [15]. Conditions of tilt are met, for example, when surface scanning manually or when using special probe designs comprising coils with a specific orientation. Apart from planar testpiece applications, they arise also in tube testing with small surface coils of the motorized rotating pancake coil (MRPC) type or of the type used in array probes. In this application, a critical parameter of the inspection is the noise produced by movement of the coil through the tube, which is known as wobble. The tilt model could be useful in wobble evaluation because the coil size is small enough compared to the curvature of the tube and inspection can be modeled as a surface inspection of a plate from the same material of the tube [14].

## II. Analysis

### A. Coil of Arbitrary Shape and Position

The 3-D problem of a tilted cylindrical coil above a conductive half-space is shown in Fig. 1. The coil axis lies on the $y = 0$ plane and is tilted through an angle $\varphi$ with respect to the surface normal. This is the basic geometry from which any other coil orientation can be generated by appropriate coordinate transformations in Fourier space. The coil is wound with $N$ wire turns and is driven by a harmonically varying current $I\exp(i\omega t)$, where $\omega = 2\pi f$ and $f$ denotes the excitation frequency. The half-space is assumed to have a constant conductivity $\sigma$ and magnetic permeability $\mu = \mu_r\mu_0$.

Introducing a Cartesian coordinate system in which the plane $z = 0$ coincides with the conductor surface, two regions of interest are created:

- the air region between the bottom of the coil and the interface $0 \leq z < l_0$;
- the conductor region $z \leq 0$.

Digital Object Identifier 10.1109/TMAG.2005.854331

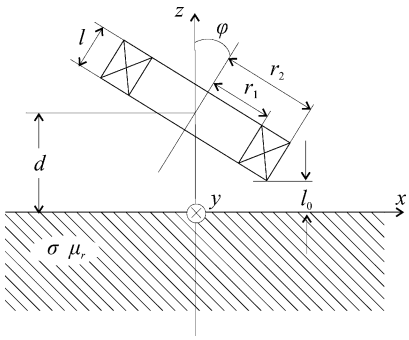


Fig. 1. Tilted cylindrical coil above a conductive half-space. The cross-sectional view shows the $y = 0$ plane.

The impedance change of any air-cored coil located above a conductive half-space is given by the general expression [2]

$$\Delta Z = 2i\omega\mu_0 \int_{-\infty}^{\infty}\int_{-\infty}^{\infty} \frac{1}{a}\tilde{h}^{(s)}(-u,-v)\tilde{h}^{(s)}(u,v)\frac{\mu_r a - a_1}{\mu_r a + a_1}\mathrm{d}u\,\mathrm{d}v \tag{1}$$

where $a = \sqrt{u^2+v^2}$ and $a_1 = \sqrt{a^2 + i\omega\mu_r\mu_0\sigma}$ and the source term $\tilde{h}^{(s)}$ is the 2-D Fourier transform of the normal component of the free-space magnetic field incident on the surface $z = 0$

$$\tilde{h}^{(s)}(u,v) = \frac{1}{2\pi I}\int_{-\infty}^{\infty}\int_{-\infty}^{\infty} H_z^{(s)}(x,y,z=0)\exp(-iux) \times \exp(-ivy)\mathrm{d}x\,\mathrm{d}y. \tag{2}$$

The other term in the integrand of (1) is a reflection coefficient representing the effect of the conductive half-space and is modified accordingly for the case of a plate [3] or a layered conductor. Since (2) involves a Fourier transform of a real function, we can write $\tilde{h}^{(s)}(-u,-v) = \tilde{h}^{(s)}(u,v)^*$ and, therefore, reduce the integration intervals to positive $u$ and $v$ so that the impedance change can be calculated from

$$\Delta Z = i8\omega\mu_0 \int_0^{\infty}\int_0^{\infty} \frac{1}{a}\left|\tilde{h}^{(s)}(u,v)\right|^2 \frac{\mu_r a - a_1}{\mu_r a + a_1}\mathrm{d}u\,\mathrm{d}v. \tag{3}$$

Likewise, we can calculate the induced eddy-current density

$$\mathbf{J} = \frac{\omega\sigma\mu_0\mu_r I}{\pi}\int_{-\infty}^{\infty}\int_{-\infty}^{\infty} \tilde{h}^{(s)}(u,v)\frac{1}{a(a\mu_r + a_1)}(v\hat{\mathbf{x}} - u\hat{\mathbf{y}}) \times \exp(a_1 z)\exp(iux)\exp(ivy)\mathrm{d}u\,\mathrm{d}v \tag{4}$$

and the magnetic field inside ($z \le 0$)

$$\mathbf{H} = \frac{I}{\pi}\int_{-\infty}^{\infty}\int_{-\infty}^{\infty} \tilde{h}^{(s)}(u,v)\frac{a_1}{a(a\mu_r + a_1)}(iu\hat{\mathbf{x}} + iv\hat{\mathbf{y}} + a_1\hat{\mathbf{z}}) \times \exp(a_1 z)\exp(iux)\exp(ivy)\mathrm{d}u\,\mathrm{d}v \tag{5}$$

and outside $0 \le z \le l_0$ the planar conductor

$$\mathbf{H} = \frac{I}{2\pi}\int_{-\infty}^{\infty}\int_{-\infty}^{\infty} \frac{\tilde{h}^{(s)}(u,v)}{a} \times \left\{\left[\exp(az) - \frac{a\mu_r - a_1}{a\mu_r + a_1}\exp(-az)\right](iu\hat{\mathbf{x}} + iv\hat{\mathbf{y}}) + \left[\exp(az) + \frac{a\mu_r - a_1}{a\mu_r + a_1}\exp(-az)\right]a\hat{\mathbf{z}}\right\} \times \exp(iux)\exp(ivy)\mathrm{d}u\,\mathrm{d}v. \tag{6, 7}$$

Note that eddy currents lack a vertical component, irrespective of the coil shape and orientation, and this is true not only on the surface but also throughout the entire conductor volume. Similar expressions can be derived using another form of the source term, which arises when using the second-order vector potential formulation [8]. Now, the aim is the calculation of $\tilde{h}^{(s)}(u,v)$ for the tilted coil of Fig. 1. This term has a closed-form expression in two symmetrical cases: the parallel coil when $\varphi = 0$ and the perpendicular coil when $\varphi = \pi/2$. From [3], the source term for the parallel coil is

$$\tilde{h}^{(s)}(u,v) = \frac{n}{2a^3}J(ar_1, ar_2)\{\exp[-a(l+l_0)] - \exp(-al_0)\} \tag{8}$$

where $n = N/[(r_2 - r_1)l]$ is the turns density and

$$J(x_1,x_2) = \int_{x_1}^{x_2} xJ_1(x)\mathrm{d}x = \frac{\pi}{2}\{x_1[J_0(x_1)\mathbf{H}_1(x_1) - J_1(x_1)\mathbf{H}_0(x_1)] - x_2[J_0(x_2)\mathbf{H}_1(x_2) - J_1(x_2)\mathbf{H}_0(x_2)]\} \tag{9}$$

where $J_n$ and $\mathbf{H}_n$ denote Bessel and Struve functions, respectively, of order $n$. Substituting (8) in (3) and using Hankel transform identities, we can derive the classical integral expression for the impedance change of the axisymmetrically positioned cylindrical coil [17]. From [3], the source term for the perpendicular coil is

$$\tilde{h}^{(s)}(u,v) = in\exp(-ad)\sin\frac{ul}{2}M(ur_1, ur_2)u^{-3} \tag{10}$$

where

$$M(x_1,x_2) = \int_{x_1}^{x_2} xI_1(x)\mathrm{d}x = \frac{\pi}{2}\{x_1[I_0(x_1)\mathbf{L}_1(x_1) - I_1(x_1)\mathbf{L}_0(x_1)] - x_2[I_0(x_2)\mathbf{L}_1(x_2) - I_1(x_2)\mathbf{L}_0(x_2)]\} \tag{11}$$

and $I_n$ and $\mathbf{L}_n$ denote modified Bessel and Struve functions, respectively, of order $n$.

### *B. The Tilted Coil*

For intermediate tilt angles $0 < \varphi < \pi/2$, we can use a numerical method for computing $\tilde{h}^{(s)}(u,v)$, which is based on a numerical calculation of the free-space coil field $H_z^{(s)}(x,y,z=0)$ and the use of two-dimensional fast Fourier transform (2-D

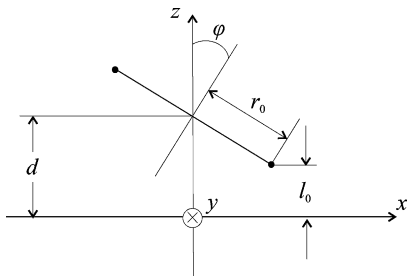


Fig. 2. Tilted filamentary circular loop in free-space. The cross-sectional view shows the $y = 0$ plane.

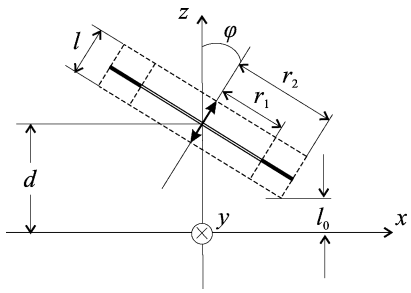


Fig. 3. Tilted flat coil in free-space. The cross-sectional view shows the $y = 0$ plane. The final coil cross section after superposition is also shown as a dashed outline.

FFT) routines [13]. In this case, the computational burden is the calculation of the magnetic field but the computation can be significantly accelerated by using special expressions derived from the Biot–Savart law [18] and coordinate transformations to account for the tilt. Although this approach seems to be appropriate for complex coil shapes it is not necessary for the tilted cylindrical coil since in this case we can also derive an analytical expression, starting from a relevant result for a filamentary tilted current loop. Consider Fig. 2, where a loop of radius $r_0$ and excitation current $I$ is positioned so that it can be rotated around its center at $(x_0, y_0, z_0) = (0, 0, d)$.

Following [11], where the isolated filamentary circular loop coil produces a magnetic flux density in the region below the coil $z < l_0$

$$B_z(x,y,z) = \frac{i\mu_0 r_0 I}{4\pi} \int_{-\infty}^{\infty}\int_{-\infty}^{\infty} I_1(\psi r_0)\exp[a(z-d)] \times \exp(iux)\exp(ivy)\mathrm{d}u\,\mathrm{d}v \quad (12)$$

where $d = l_0 + r_0 \sin|\varphi|$ and $\psi = u\sin\varphi + ja\cos\varphi$ with angle $\varphi$ taken positive for a clockwise rotation and negative for an anticlockwise rotation. This result was obtained using the magnetic vector potential and a geometric technique where the filamentary loop is considered as the intersection of two surfaces. A similar result was obtained in [10] using coordinate transformations in Fourier space. From (12) and (2), the source term for the filamentary loop is

$$\tilde{h}^{(s)}(u,v) = \frac{ir_0}{2} I_1(\psi r_0)\exp(-ad). \quad (13)$$

The procedure to find the source term for the rectangular cross-section coil of Fig. 1 involves two superposition steps.

- Step 1: from filamentary to flat coil.

  The first superposition is performed in terms of the filamentary coil radius $r_0$ in order to find the source term for the flat coil of Fig. 3. This involves integration of the term $r_0 I_1(\psi r_0)$ from the inner to the outer radius of the flat coil and the result is

  $$\tilde{h}^{(s)}(u,v) = \frac{in_f}{2}\frac{M(\psi r_1, \psi r_2)}{\psi^2}\exp(-ad) \quad (14)$$

  where now $d = l_0 + r_2 \sin|\varphi|$ and $n_f$ is the turns density of the flat coil.
- Step 2: from flat to finite cross-section coil.

  The second superposition is performed along the axis of the flat coil (the range of integration is depicted by the bold arrow in Fig. 3). When a new flat coil is displaced by $\Delta l$ along its axis, its center lies at the point $(x_0, y_0, z_0) = (\Delta l \sin\varphi, 0, d + \Delta l\cos\varphi)$, where now $d = l_0 + r_2\sin|\varphi| + (l/2)\cos\varphi$. The source term is written as

  $$\tilde{h}^{(s)}(u,v)\exp(iu\Delta l\sin\varphi)\exp(-a\Delta l\cos\varphi) = \tilde{h}^{(s)}(u,v)\exp(i\psi\Delta l) \quad (15)$$

  where $\tilde{h}^{(s)}(u,v)$ is taken from (14). The source term for the coil of Fig. 1. is obtained by integrating $\Delta l$ from $-l/2$ to $+l/2$. The dashed outline in Fig. 3 shows the final coil cross section. The result is

  $$\tilde{h}^{(s)}(u,v) = in\frac{M(\psi r_1, \psi r_2)}{\psi^3}\exp(-ad)\sin\left(\frac{\psi l}{2}\right). \quad (16)$$

  After substituting (16) in (3), we get the expression for the impedance change

  $$\Delta Z = i8\omega\mu_0 n^2 \int_0^{\infty}\int_0^{\infty} \frac{\exp(-2ad)}{a} \times \left|\frac{M(\psi r_1, \psi r_2)}{\psi^3}\sin\left(\frac{\psi l}{2}\right)\right|^2 \frac{\mu_r a - a_1}{\mu_r a + a_1}du\,dv. \quad (17)$$

  The total impedance of the coil is the sum of the isolated coil impedance $Z_0$ and the change $\Delta Z$ produced by the eddy currents induced in the planar conductor. The expression for $Z_0$ is given in [17].

Any other cylindrical coil arrangement can be modeled beginning with the basic configuration of the tilted coil and applying 2-D Fourier identities for the skewed and shifted functions. Thus, if the coil is rotated around the $z$ axis by an angle $\chi$ and shifted so that its center lies above $(x_0, y_0)$, the new source term is calculated from the old one by

$$\tilde{h}_z^{(s)}(u\cos\chi + v\sin\chi, -u\sin\chi + v\cos\chi) \times \exp(iux_0)\exp(ivy_0). \quad (18)$$

### C. $\Delta Z$ for an Infinitely Long Crack

In order to investigate the effect of tilt on flaw detection, we use an approximate analytical and yet quite accurate model of crack inspections, which is the thin-skin theory developed in

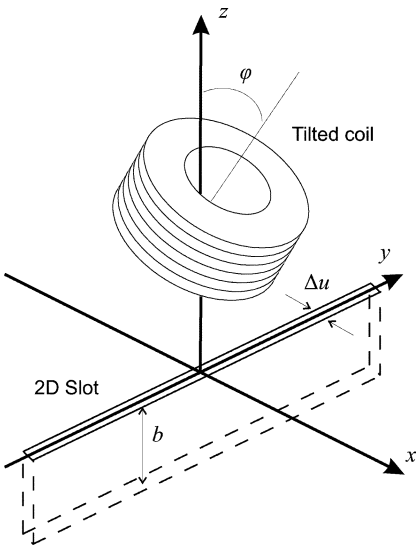


Fig. 4. Tilted coil above a long slot.

[16]. Here we use it in a compact form presented in [19] for long cracks, after slightly modifying it so that the incident coil magnetic field appears in the equations instead of the incident magnetic potential. Referring to Fig. 4, the impedance change produced by the long slot $\Delta Z^c$, which is filled with air, is calculated from

$$\Delta Z^c = \frac{\mu_0 \omega}{2\pi} \int_{-\infty}^{\infty} \frac{g}{1 + 2\left(\frac{v}{ik}\right)\tilde{U}\tanh(vb)} \frac{\tilde{H}_y(-v)\tilde{H}_y(v)}{v^2} \mathrm{d}v \tag{19}$$

where $g$ and $\tilde{U}$ are given in the Appendix. In (19), the contribution of the coil is described by the source term

$$\tilde{H}_y(v) = \frac{1}{I} \int_{-\infty}^{\infty} H_y(x = 0, y, z = 0) \exp(-ivy) \mathrm{d}y \tag{20}$$

which is the Fourier transform of the $y$ component of the magnetic field at the crack mouth when the crack is absent. All other terms in (19) are coil independent and are given in the Appendix. In the tilted coil case of Fig. 4, we can deduce the expression for $\tilde{H}_y(v)$ from (16) and (6) or (5)

$$\tilde{H}_y(v) = iv \int_{-\infty}^{\infty} \frac{M(\psi r_1, \psi r_2)}{a\psi^3} \exp(-ad) \times \sin\left(\frac{\psi l}{2}\right) \frac{a_1}{a\mu_r + a_1} \mathrm{d}u. \tag{21}$$

Equation (21) can be modified using again (18) for a rotated and shifted coil. It has to be emphasized that the crack model is valid in the limit of small skin depth (high frequency regime) and for: 1) closed cracks (zero gap) in both magnetic and nonmagnetic half-space for all coil configurations; 2) open cracks (small gap) in nonmagnetic half-space again for all coil configurations; and 3) open cracks in magnetic half-space only for symmetric coils and coil positions; see discussion in [16]. In the cylindrical tilted coil configuration, the last case, which is the limiting one, accounts for arbitrary coil tilt provided that $x_0 = 0$ and $\chi = \pi/2$ in (18). The model is applicable to most surface crack inspections since these are operated at very high frequencies and the cracks do have a negligible opening.

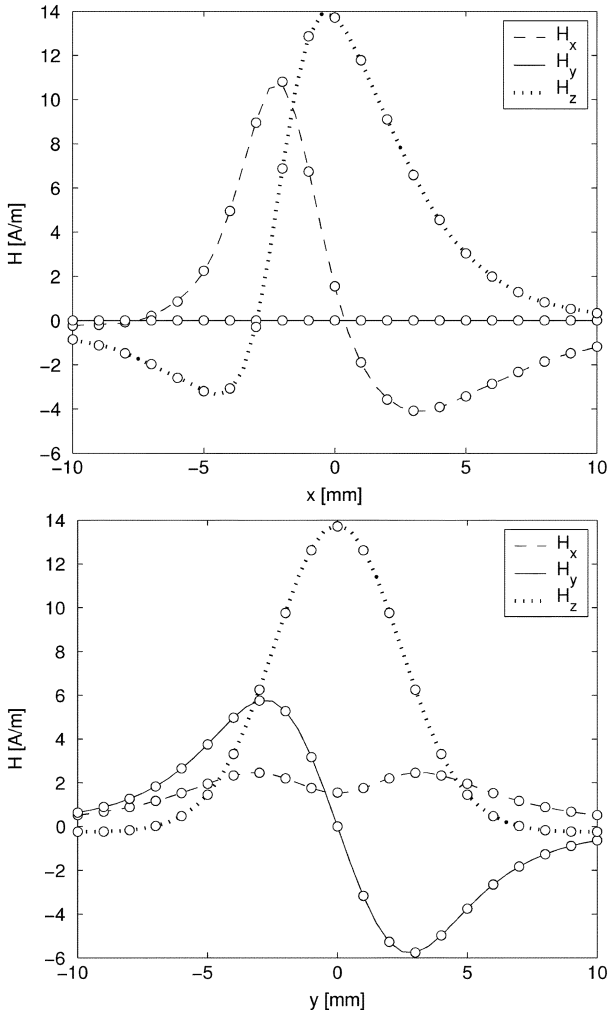


Fig. 5. Free-space magnetic field in the area underneath the tilted coil ($\varphi = 45°$). Comparison of results from the presented model (solid curves) and Biot–Savart computations (circles).

TABLE I
TEST PARAMETERS FOR THE NUMERICAL COMPUTATIONS IN FIGS. 5–8

| Coil | | Testpiece | |
|---|---|---|---|
| $r_1$ | 2 mm | $\sigma$ | 18.72 MS/m |
| $r_2$ | 4 mm | $\mu_r$ | 1 |
| $l$ | 2 mm | | |
| $l_0$ | 1 mm | | |
| $N$ | 400 | | |

## III. RESULTS

### A. Numerical Aspects and Corroboration

An important numerical aspect of the solution is the computation of the integral in (11), which is also present in (16) but

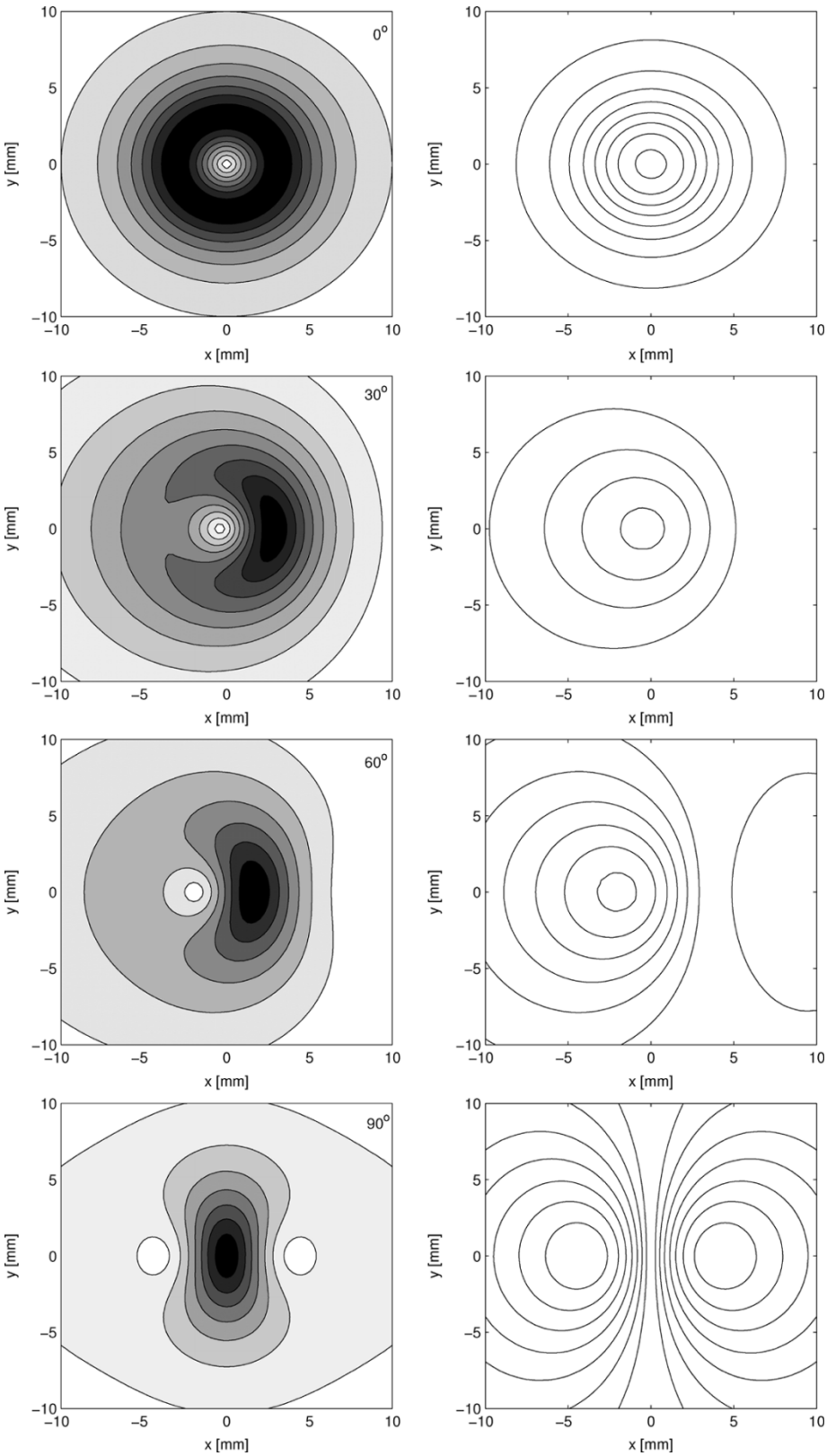


Fig. 6. Amplitude contours (left) and streamlines (right) of eddy currents induced on the surface of a conductive half-space by a cylindrical coil at various tilt angles. Coil rotation is clockwise.

with a complex argument. We can avoid the computation of the complex modified Struve function by using the identity

$$\int_{z_1}^{z_2} I_1(z) z dz = z_2 I_0(z_2) - z_1 I_0(z_1) - \int_{z_1}^{z_2} I_0(z) dz \qquad (22)$$

and then compute the integral in (22) by the very fast converging series [20]

$$\int_{z_1}^{z_2} I_0(z) dz = 2 \sum_{k=0}^{\infty} (-1)^k [I_{2k+1}(z_2) - I_{2k+1}(z_1)]. \qquad (23)$$

Moreover, the term $\sin(\psi l/2)$ in (16) may cause overflow if automatic integration routines are used and $u$ and $v$ take very large values. The problem is overcome by making the following substitution in (16) that results in a more stable numerical scheme:

$$\exp(-ad)\sin\left(\frac{\psi l}{2}\right) = \frac{\exp\left(\frac{i\psi l}{2} - ad\right) - \exp\left(-\frac{i\psi l}{2} - ad\right)}{2i}. \tag{24}$$

Since the model described by (1) has been extensively validated [2]–[4], we only need to verify the correctness of the source term expression. Thus, we need only investigate whether we get correct results for the free-space magnetic field using (16) and (6) with $\sigma = 0$. Fig. 5 shows the variation of the magnetic field components along the $x$ and $y$ axes for coil data as in Table I and tilt angle $\varphi = 45°$. The results are compared to numerical ones derived with Biot–Savart numerical calculations [18] and the agreement is excellent.

In addition, a useful check is whether (16) reduces either to (8) or to (10) for the relevant tilt angles. Indeed, this is trivial for (10) when $\varphi = \pm\pi/2$ since $\psi = \pm u$ and it is straightforward for (8) when $\varphi = 0$ since $\psi = ia$ and $M(iar_1, iar_2) = iJ(ar_1, ar_2)$.

### *B. Eddy Currents and Coil Impedance*

Computation of the eddy-current density from (4) is facilitated by the use of 2-D FFT routines. Fig. 6 shows amplitude contours and streamlines or surface eddy currents at four tilt angles. The streamlines are contour plots of a scalar function $\phi$ where $\mathbf{J} = \nabla \times (\phi\hat{\mathbf{z}})$ and the expression for $\phi$ can be easily deduced from (4). For a parallel coil, eddy currents flow on circular paths while for the perpendicular coil eddy-current flow is uniform underneath the coil but tends to a circular pattern on either side of the coil faces. We note that the flow patterns for the other two tilt angles have an intermediate form comparing to the parallel and perpendicular ones. As expected, eddy-current density is stronger on the side where the coil is closer to the conductive half-space.

In double precision arithmetic, the CPU time for the computation of such a pattern on a typical Pentium IV PC is about 1 s. About the same time is also needed for the computation of a single impedance value. Fig. 7 shows the impedance change of the coil as a function of tilt angle with $l_0$ kept constant and the same information is presented on the impedance plane of Fig. 8, which plots normalized probe inductive reactance change versus normalized probe resistance change. Following the usual practice in eddy-current NDI, the impedance is normalized to the reactance of the coil in free-space $X_0$. The tilt curves are computed at four distinct frequencies, and from Fig. 7 we observe the decrease of impedance change with tilt angle due to the weaker electromagnetic coupling of the coil with the conductive half-space. This is expected because $d$ increases with the tilt angle. However, we observe a weak minimum in $\Delta R$ and $\Delta X$ around 70°. This is a consequence of the finite height of the coil and the fact that the maximum in $d$ does not occur at 90° but at a smaller angle. From Fig. 8 we observe that the tilt

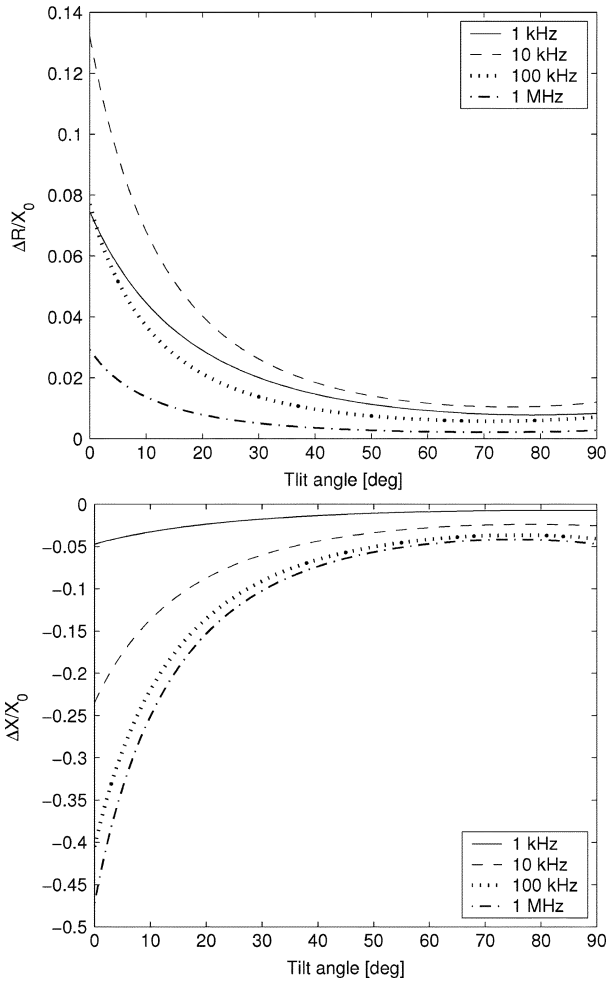


Fig. 7. Normalized resistive and reactive component of the impedance change as a function of tilt angle.

curves are almost straight lines and have a strong resemblance to lift-off curves, with which they share the same phase. The constant phase signal is produced by any coil position or orientation change and it is characteristic of eddy-current testing. As a result, any other signal of different phase will indicate the change of another parameter such as the change of $\sigma$ or $\mu_r$ or the presence of a flaw. This phase discrimination technique is very common in eddy-current inspection and is routinely applied by rotating the impedance display in the eddy-current instrument screen so that lift-off and tilt signals are positioned horizontally and any vertical deflection accounts for flaws.

### *C. Crack Inspection*

Fig. 9 shows the variation of $\Delta Z^c$ with tilt angle for the coil and test parameters shown in Table II. For each tilt angle, the coil is centered above the crack and $l_0$ is kept constant. For the cylindrical coil this variation is not linear, with abrupt changes taking places at small angles. The larger the tilt angle, the smaller the impedance change owing to the crack due again to the weaker electromagnetic coupling of the coil with the conductive half-space. In the limit of a perpendicular coil, $\Delta Z^c$ becomes zero because in this case $H_y(0, y, 0) = 0$ or equivalently the eddy currents are not obstructed by the crack. Note also that for the

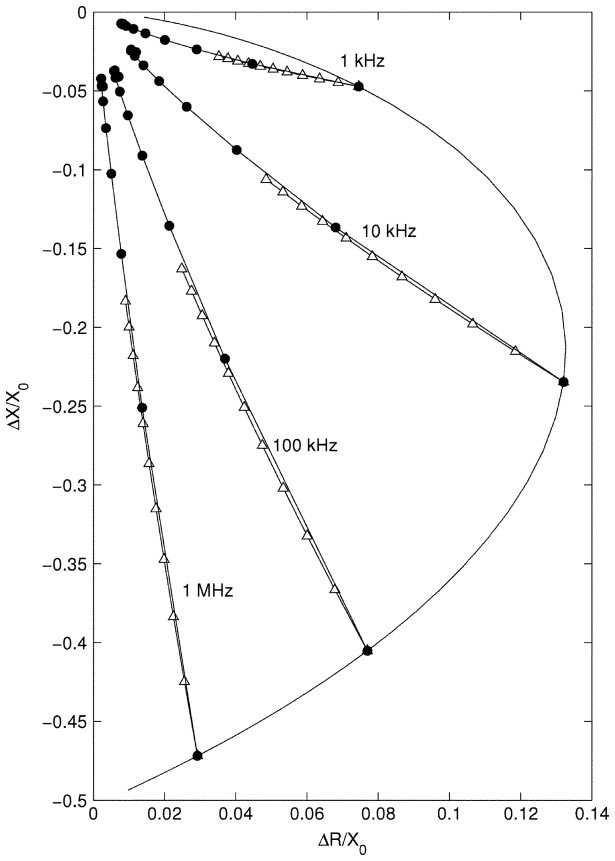


Fig. 8. Impedance change display showing tilt (•) and lift-off curves (△) in steps of 10° and 0.1 mm, respectively. The arc-shaped curve is produced by varying excitation frequency at zero lift-off and zero tilt angle.

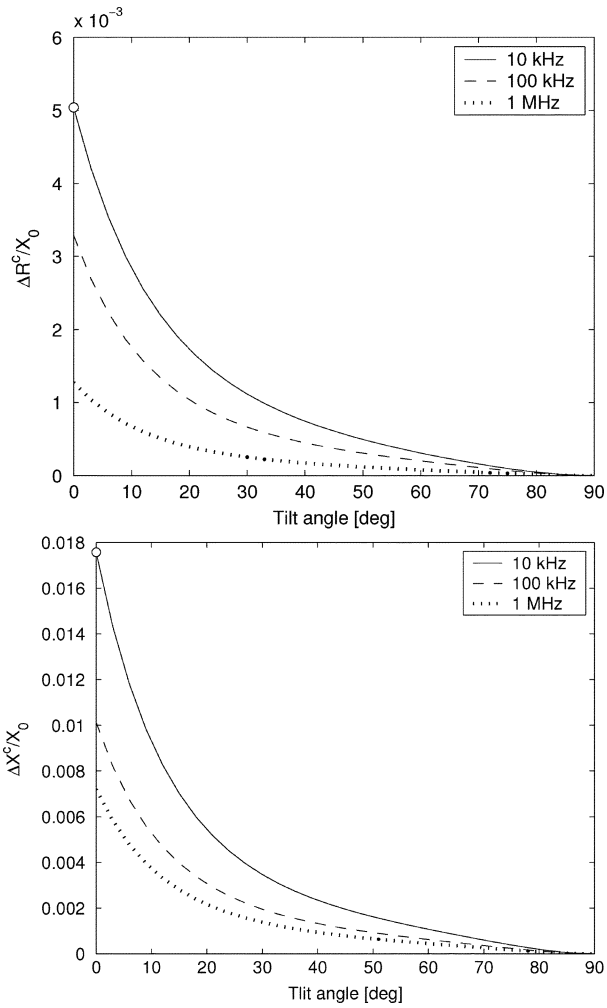


Fig. 9. Normalized resistive and reactive component of the impedance change due to the crack as a function of tilt angle. The circles for zero tilt angle are experimental measurements.

same tilt angle the tilt signal increases with frequency while the crack signal decreases so that the signal-to-noise ratio decreases. This is a well-known feature of eddy-current testing and the usual countermeasures taken, after rotating the impedance display and putting the tilt noise signal on the horizontal, are filtering or attenuation of the horizontal noise signal or display of only the vertical signal.

A realistic model, however, should assume the simultaneous change of coil position and tilt. In this case only a small tilt of the order of a degree is enough to disturb the form of the crack signal as the coil is moved above the crack. The added crack and tilt impedance change signals, as the coil is scanned across the crack (moved along the $x$ axis), is shown in Fig. 10 for random tilt angle variation of $\pm 1^\circ$ and $\pm 5^\circ$ at three frequencies. The tilt variation was introduced every 2 mm of coil travel. Experimental measurements are also shown for the $\varphi = 0$ case. The disturbance of the useful crack signal from the tilt noise is more pronounced at large tilt angles and higher frequencies.

## IV. Conclusion

Closed-form expressions for the impedance of a cylindrical coil and the electromagnetic field have been derived for an eddy-current probe coil located with an arbitrary tilt angle above a conductive half-space. The theoretical results are combined with a thin-skin theory to model long crack inspection under conditions of tilt, and the result is a realistic representation of an actual eddy-current inspection that is modeled accurately and with a fast computation scheme.

TABLE II
Test Parameters for the Numerical Computations in Figs. 9 and 10

| Coil | | Testpiece | |
|---|---|---|---|
| $r_1$ | 6.88 mm | $\sigma$ | 16.53 MS/m |
| $r_2$ | 10.7 mm | $\mu_r$ | 1 |
| $l$ | 5.0 mm | $b$ | 5.96 mm |
| $l_0$ | 2.02 mm | $\Delta u$ | 0.43 mm |
| $N$ | 410 | | |

The present work can be extended in various ways such as the computation of the mutual impedance change between two cylindrical coils oriented in any possible way or between a cylindrical coil and another probe coil design, thus extending the model from a single coil working in absolute mode to differential probes and probes working in the send–receive mode. Furthermore, it is anticipated that it can be used: 1) in inverse problem studies involving either deterministic or stochastic methods for the extraction of the crack signal from the noisy background and 2) as a complementary tool to numerical methods, such as VIM, for the computation of the incident coil field in the uncracked conductor.

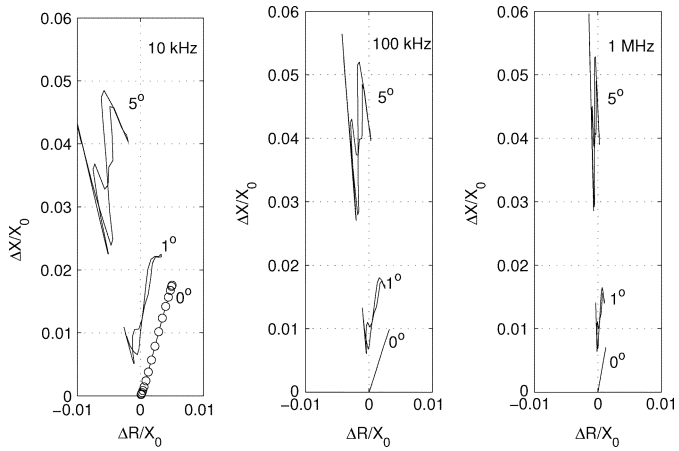


Fig. 10. Crack signals at three frequencies. Realistic representation of manual scanning by introducing a random tilt of $\pm 1^\circ$ and $\pm 5^\circ$ maximum. The circles for zero tilt and 10-kHz frequency are experimental measurements.

## APPENDIX

The following are definitions of the parameters in (19):

$$g = ig_f \Delta u + (1+i)\mu_r \delta \left( g_f - \frac{1}{2} g_s \Delta u \right) + \frac{1}{2} g_k \mu_r \delta^2 \quad (25)$$

$$g_s = g_{s0} - g_{s1} \quad (26)$$

$$g_k = -\frac{4}{\pi}(g_{s0} + g_{s2}) + g_{s1} \quad (27)$$

$$g_{s0} = \left[ 1 + 2\left( \frac{v}{ik} \right) (\tilde{U} + \tilde{V}) \tanh(vb) \right] v^2 \quad (28)$$

$$g_f = v \tanh(vb) \quad (29)$$

$$g_{s1} = v^2 \operatorname{sech}(vb) \quad (30)$$

$$g_{s2} = v^2. \quad (31)$$

For a magnetic half-space material, the functions $\tilde{U}(v)$ and $\tilde{V}(v)$ are computed from

$$\tilde{U}(v) = \frac{\mu_r}{2\pi \left[ (\mu_r^2 - 1) w^2 + \mu_r^2 \right]} \left[ \frac{\mu_r}{w} \ln \left( \frac{1+w}{1-w} \right) - \frac{1}{\sqrt{1+w^2}} \times \ln \left( \frac{1+\sqrt{1+w^2}}{1-\sqrt{1+w^2}} \right) + \frac{\mu_r^2 - 1}{\sqrt{(\mu_r^2 - 1) w^2 + 1}} \times \ln \left( \frac{\sqrt{(\mu_r^2 - 1) w^2 + 1} + \mu_r}{\sqrt{(\mu_r^2 - 1) w^2 + 1} - \mu_r} \cdot \frac{\sqrt{(\mu_r^2 - 1) w^2 + 1} - 1}{\sqrt{(\mu_r^2 - 1) w^2 + 1} + 1} \right) \right] \quad (32)$$

$$\tilde{V}(v) = -\frac{\mu_r}{2\pi \sqrt{(\mu_r^2 - 1) w^2 + 1}} \ln \left( \frac{\sqrt{(\mu_r^2 - 1) w^2 + 1} + \mu_r}{\sqrt{(\mu_r^2 - 1) w^2 + 1} - \mu_r} \times \frac{\sqrt{(\mu_r^2 - 1) w^2 + 1} - 1}{\sqrt{(\mu_r^2 - 1) w^2 + 1} + 1} \right) \quad (33)$$

where $w = v/k$ and $k = (-1+i)/\delta$ with $\delta = \sqrt{2/(\omega \mu_0 \mu_r \sigma)}$ denoting the electromagnetic skin depth. For nonmagnetic half-space material, (32) and (33) should reduce to

$$\tilde{U}(v) = \frac{1}{2\pi} \left[ \frac{1}{w} \ln \left( \frac{1+w}{1-w} \right) - \frac{1}{\sqrt{1+w^2}} \ln \left( \frac{1+\sqrt{1+w^2}}{1-\sqrt{1+w^2}} \right) \right] \quad (34)$$

$$\tilde{V}(v) = -\frac{\mu_r}{2\pi} \ln \left( \frac{w^2}{\sqrt{w^2 - 1}} \right). \quad (35)$$

## ACKNOWLEDGMENT

The author is grateful to Dr. S. K. Burke, Defence Science and Technology Organization, Australia, for providing the experimental data and suggestions on improving the manuscript.

## REFERENCES

[1] T. P. Theodoulidis, "Modeling of homogeneous conducting media," in *Nondestructive Testing Handbook*, 3rd ed, R. C. McMaster *et al.*, Eds: American Society for Nondestructive Testing, 2004, vol. 5, pp. 65–73.

[2] S. K. Burke, "Eddy current induction in a uniaxially anisotropic plate," *J. Appl. Phys.*, vol. 68, pp. 3080–3090, 1990.

[3] S. K. Burke and M. E. Ibrahim, "Mutual impedance of air-cored coils above a conducting plate," *J. Phys. D, Appl. Phys.*, vol. 37, pp. 1857–1868, 2004.

[4] S. K. Burke, "Impedance of a horizontal coil above a conducting half-space," *J. Phys. D, Appl. Phys.*, vol. 19, pp. 1159–1173, 1986.

[5] J. R. Bowler, "Eddy current calculations using half-space Green's functions," *J. Appl. Phys.*, vol. 61, no. 3, pp. 833–839, 1987.

[6] J. R. Bowler and V. Katyal, "Magnetic sensor array for eddy current field measurement with a racetrack coil excitation," *Electromagn. Nondestruct. Eval. (VIII)*, pp. 36–43, 2004.

[7] J. Zhou, R. Collins, and D. H. Michael, "Half-space induction by a rectangular coil with rounded corners: Local uniformity and ACFM," *Rev. Progr. Quant. Nondestruct. Eval.*, vol. 13, pp. 335–342, 1994.

[8] T. P. Theodoulidis and E. E. Kriezis, "Impedance evaluation of rectangular coils for eddy current testing of planar media," *NDT&E Int.*, vol. 35, pp. 407–414, 2002.

[9] E. E. Kriezis and I. E. Xypteras, "Eddy current distribution and loss in a semi-infinite conducting plate," *ETZ Archiv*, vol. 7, pp. 201–207, 1979.

[10] R. E. Beissner and M. J. Sablik, "Theory of eddy currents induced by a nonsymmetric coil above a conducting half-space," *J. Appl. Phys.*, vol. 56, no. 2, pp. 448–454, 1984.

[11] H. J. Tsaknakis and E. E. Kriezis, "Field distribution due to a circular current loop placed in an arbitrary position above a conducting plate," *IEEE Trans. Geosci. Remote Sens.*, vol. GRS-23, pp. 834–840, 1985.

[12] S. M. Panas and A. G. Papayiannakis, "Eddy currents in an infinite slab due to an elliptic current excitation," *IEEE Trans. Magn.*, vol. 27, no. 5, pp. 4328–4337, Sep. 1991.

[13] S. H. Sadeghi and A. H. Salemi, "Electromagnetic field distributions around conducting slabs, produced by eddy current probes with arbitrary shape current carrying excitation loops," *Proc. Inst. Elect. Eng.—Sci., Meas. Technol.*, vol. 148, no. 4, pp. 187–192, 2001.

[14] M. Mayos, S. Mastorchio, L. Aubry, and K. Miya, "Simulation of the behavior of Cecco probes to lift-off and tilt effects during tube inspection," *Electromagn. Nondestruct. Eval. (III)*, pp. 208–216, 1999.

[15] R. Albanese, R. Baresi, M. Carbone, and A. Gasparics, "Tools for the design of fluxset probes addressed to the detection of deep defects," *Electromagn. Nondestruct. Eval. (VIII)*, pp. 52–57, 2004.

[16] N. Harfield and J. R. Bowler, "Theory of thin-skin eddy-current interaction with surface cracks," *J. Appl. Phys.*, vol. 82, no. 6, pp. 4590–4603, 1997.

[17] C. V. Dodd and W. E. Deeds, "Analytical solutions to eddy current probe coil problems," *J. Appl. Phys.*, vol. 39, no. 6, pp. 2829–2838, 1968.

[18] K. L. Forbes, S. Crozier, and D. M. Doddrell, "Rapid computation of static fields produced by thick circular solenoids," *IEEE Trans. Magn.*, vol. 33, no. 5, pp. 4405–4410, Sep. 1997.

[19] R. J. Ditchburn, S. K. Burke, and M. Posada, "Eddy-current nondestructive inspection with thin spiral coils: Long cracks in steel," *J. Nondestruct. Eval.*, vol. 22, no. 2, pp. 63–77, 2003.

[20] I. S. Gradshteyn and I. M. Ryzhik, *Table of Integrals Series and Products*, 6th ed. New York: Academic, 2000, p. 653.

Manuscript received March 15, 2005; revised June 6, 2005.